



Article

Tungsten-Doped VO₂/Starch Derivative Hybrid Nanothermochromic Hydrogel for Smart Window

Yu Wang¹, Fang Zhao^{1,*} , Jie Wang^{1,*}, Li Li¹, Kaiqiang Zhang², Yulin Shi², Yanfeng Gao^{3,4,*} and Xuhong Guo^{1,2} 

¹ State Key Laboratory of Chemical Engineering, East China University of Science and Technology, Shanghai 200237, China

² Engineering Research Center of Materials Chemical Engineering of Xinjiang Bingtuan, Key Laboratory of Materials Chemical Engineering of Xinjiang Uygur Autonomous Region, Shihezi University, Shihezi 832000, China

³ School of Materials Science and Engineering, Shanghai University, Shanghai 200444, China

⁴ School of Materials Science and Energy Engineering, Foshan University, Foshan 528000, China

* Correspondence: Fzhaol@ecust.edu.cn (F.Z.); jiewang2010@ecust.edu.cn (J.W.); yfgao@shu.edu.cn (Y.G.); Tel.: +86-21-64253488 (F.Z.); +86-21-64253491 (J.W.); +86-21-66138005 (Y.G.)

Received: 25 May 2019; Accepted: 27 June 2019; Published: 2 July 2019



Abstract: Highly efficient energy-saving windows with high solar modulation properties (ΔT_{sol}) are the everlasting pursuit of research for industrial applications in the smart window field. Hybridization is an effective means of improving both ΔT_{sol} and luminous transmittance (T_{lum}). In this paper, hybrid thermochromic films were synthesized using tungsten-doped VO₂ nanoparticles (NPs) and starch derivatives. Thermoresponsive 2-hydroxy-3-butoxypropyl starch (HBPS) was prepared with a low critical solution temperature (LCST) varying from 32 to 21 °C by the substitution of reactive groups. The hybrid film was obtained by dispersing W-doped VO₂ NPs in HBPS hydrogels, which exhibiting remarkable solar modulation property ($\Delta T_{\text{sol}} = 34.3\%$) with a high average luminous transmittance ($T_{\text{lum, average}} = 53.9\%$).

Keywords: W-doped VO₂ (M) NPs; starch derivative; inorganic and organic hybrid film; thermochromism; smart window

1. Introduction

Facilities in buildings including heating, ventilation, and air conditioning use most of the world's energy [1]. Around the world, 40% of building's energy consumption is attributed to air conditioning [2], which induces a series of problems. Reducing the energy consumption of these facilities while maintaining the comfort level is one of the biggest challenges in the sustainable development of buildings [3]. One effective way to improve a building's energy efficiency is coating the glass with chromogenic materials such as electrochromic, gasochromic, and thermochromic materials to obtain "smart windows" [4–10]. Among these materials, thermochromic smart windows show advantages over others, mainly because they can regulate the solar transmittance in a temperature-responsive manner without extra energy input.

Vanadium dioxide (VO₂) is a commonly used inorganic thermochromic material in smart window systems. It undergoes a reversible insulator–metal transition at a critical temperature of 68 °C with a huge optical transmittance change in the infrared range (IR) [3]. Chen et al. [11] synthesized the high crystalline-quality VO₂ nanoparticles (NPs) through a "heating-up" process, which showed a high solar modulating ability ($\Delta T_{\text{sol}} = 22.3\%$). In the meantime, organic thermosensitive polymers are also favorable for the smart window system, such as poly (*N*-isopropylacrylamide), i.e., PNIPAm,

which is a hydrogel whose phase transition from a swollen state to aggregated state results in a prominent visual difference at its lower critical solution temperature (LCST, the temperature at 50% of the initial transmittance) [12]. By tuning the thickness of the PNIPAm hydrogel layer, Zhou et al. [13] obtained a smart window system based on pure PNIPAm film showing excellent solar modulating ability ($\Delta T_{\text{sol}} = 25.5\%$) with a high luminous transmittance ($T_{\text{lum}} = 70.7\%$). For the sealing problem of PNIPAm hydrogel-based smart windows, a co-solvent method was introduced in our previous work [14]. Although VO₂ and thermoresponsive polymers are the most investigated materials in smart window systems, requirements for their commercialization have not yet been totally achieved. The purpose of efficient smart windows is to maximize energy saving by increasing the T_{lum} and ΔT_{sol} values, but smart windows made from pure VO₂ or pure PNIPAm hydrogel could not meet the actual demands.

In 2015, Long et al. integrated inorganic VO₂ with PNIPAm for the first time, and thus opened up a new research direction for smart window systems [15]. To the best of our knowledge, this hybrid thermochromic film achieved the highest ΔT_{sol} (35%) in the literatures reported so far. Similarly, the ligand exchange thermochromic system was coupled with VO₂ NPs, resulting in a hybrid film that gave almost unchanged T_{lum} values after the phase transition ($T_{\text{lum, low}} = 73.36\%$ and $T_{\text{lum, high}} = 68.71\%$) with relatively high ΔT_{sol} values [16]. Although the hybridizing process offers both a larger visible and IR modulating ability, the high critical temperature of VO₂ in the polymer matrix still restricts its application in smart windows. Doping by tungsten can significantly reduce the critical temperature of VO₂ and solve the above problem [17]. Much effort has been made to investigate the effect of W doping on the phase transition temperature of VO₂. By the thermolysis method, a critical temperature decrease of 20 K per at % W in VO₂ nanopowders was achieved by Peng et al. [18]. Chen et al. reported a critical temperature reduction of 8 K per at % W using a “heating-up” method [11], and Zhao et al. synthesized V_{0.99}W_{0.01}O₂ with a decreasing gradient of 20 K per at % W [19].

Previously, a smart window film based on thermoresponsive and pH-responsive starch derivatives has been reported [20]. In this work, tungsten-doped VO₂/starch derivatives hybrid thermochromic films were obtained through a facile way. Firstly, temperature-responsive 2-hydroxy-3-butoxypropyl starch (HBPS) was successfully obtained through an etherification reaction. The LCST of these starch derivatives can be easily tuned by varying the degree of substitution of reactive groups to meet the different practical demands. Secondly, a near-room temperature hybrid thermochromic composite (LCST of HBPS was ~32 °C and the critical temperature of W-doped VO₂ was ~40 °C) was synthesized, which can maximize energy saving. Thirdly, the solar modulating ability (ΔT_{sol}), especially the IR modulating ability (ΔT_{IR}), was improved by hybridizing HBPS with W-doped VO₂ NPs.

2. Materials and Methods

2.1. Materials

Soluble starch, sodium tungstate, and NaOH were purchased from Sinopharm Chemical Reagent Co, Ltd. (Shanghai, China). Butyl glycidyl ether (BGE, 96%) and 3-(trimethoxysilyl) propyl methacrylate (KH570, 98%) were obtained from the Tokyo Chemical Industry Co., Ltd. (Tokyo, Japan). Polyvinyl pyrrolidone (PVP, K30, Mw = 58,000 g/mol) purchased from Aladdin Reagent (Shanghai, China) Co., Ltd. V₂O₅ (99.6%) was purchased from Sigma-Aldrich. H₂C₂O₄·2H₂O (AR, 99%) was purchased from Chron Chemical Reagent Co, Ltd. (Sichuan, China). Polyurethane (PU, DISPERCOLL U54) was purchased from Bayer AG (Leverkusen, Germany). All the reagents were used without further purification.

2.2. Preparation of HBPS and HBPS Hydrogel Films

Temperature-responsive starch HBPS was synthesized through an etherifying reaction between soluble starch and BGE in aqueous solution. The general synthetic route for the preparation of HBPS is presented as follows. Soluble starch of 4.05 g was suspended in the aqueous solution in a 100-mL

three-necked flask; then, 0.5 g of NaOH particles were added to the above mixture, and the resultant mixture was heated to 75 °C in the water bath. One hour later, a certain amount of BGE was added to the flask. The reaction was carried out at 75 °C for 5 h followed by neutralizing the reaction mixture to pH 7.0 [21]. The degree of substitution (DS) by BGE groups in soluble starch was calculated from ^1H NMR data (Table 1) using the following equation:

$$DS = \frac{I_{\text{CH}_3}/3}{I_{\text{H1}}} \quad (1)$$

where I_{CH_3} is the integral for the methyl group peak of the BGE group at 0.8 ppm (Peak c in Figure 1a), and I_{H1} is the integral for the anomeric proton of the starch backbone between 5.1–5.4 ppm (Figure 1a).

Table 1. Description of the two different starch derivative hydrogels prepared in this work.

Sample	BGE:AGU ¹	DS ²	LCST (°C) ³
HBPS-1	0.55	0.31	32
HBPS-2	0.65	0.42	21

¹ Molar ratio (AGU means anhydroglucose unit); ² DS, degree of substitution of butyl glucidyl ether (BGE) determined by ^1H NMR; ³ Determined by the UV-vis spectroscopy measurement. HBPS: 2-hydroxy-3-butoxypropyl starch, LCST: low critical solution temperature.

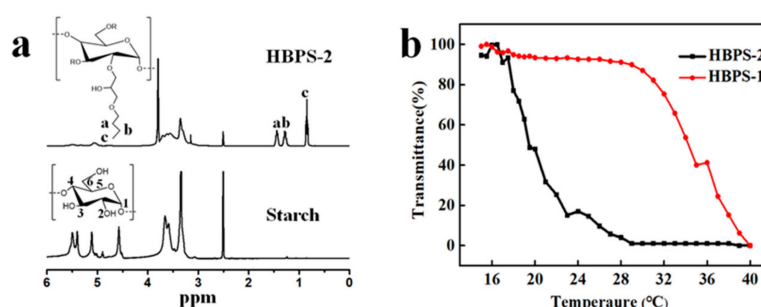


Figure 1. (a) ^1H NMR spectra of soluble starch and HBPS-2; (b) Changes of transmittance at 550 nm vs. temperature for HBPS-1 (5 g/L, $DS_{\text{BGE}} = 0.31$) and HBPS-2 (5 g/L, $DS_{\text{BGE}} = 0.42$) recorded to determine the LCST value through heating process.

The LCST value of HBPS hydrogel could be controlled by varying the dosage of BGE [22]. HBPS-1 and HBPS-2 (Table 1) with different LCST values were obtained. HBPS particles were mixed in deionized water to form HBPS hydrogel in ultrasonics for 10 min to ensure thorough dispersion. Then, HBPS hydrogel was dispersed in the glass cuvette with 3-mm thickness (Figure 2) to obtain the HBPS hydrogel films.

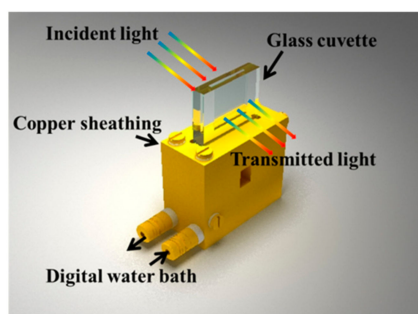


Figure 2. Schematics of the measuring device for the optical transmittance of samples.

2.3. Preparation of W-Doped VO₂ NPs and VO₂/PU Composite Film

In a typical procedure, 0.125 g of V₂O₅ powders were dispersed into 40 mL of 0.15 M of H₂C₂O₄·2H₂O to form a uniform dispersion. Then, sodium tungstate was added directly to the above dispersion as the doping agent, following by stirring for around 30 min. The pH value of the resultant dispersion was adjusted to 7 by using NaOH solution (0.1 M). A brown precursor was formed during the addition of NaOH. The precursor was collected, washed with deionized water for several times, and then dried in a vacuum oven. Then, the precursor powders were placed in a nitrogen-filled furnace to undergo the solid-state reaction at 60 °C for 10 h. The final nanoparticle product was collected, washed for three times with deionized water, and dried in a vacuum oven at 60 °C for 12 h. As reported by our previous paper [23], the critical temperature and the doping ratio exhibit a linear relationship. Thus, the actual W content in the as-prepared NPs with a phase transition temperature of 39 °C (Figure S1b) could be determined to be approximately 1.0 at %.

Then, the as-prepared W-doped VO₂ NPs (~2 wt %) were dispersed in the deionized water with continuous stirring for around 10 min, and a certain amount of the KH 570 was added followed by ultrasonic treatment for approximately 30 min. Then, PU was gradually added under stirring conditions for 20 min. Finally, the VO₂/PU composite film with a 2 to 3-μm thickness was formed by casting the above suspension on the PET (polyethylene terephthalate) substrate using an automatic coating machine (Elcometer 4340, Jerrymeter Co., Ltd., Beijing, China) equipped with grooved wire rods (groove depth 2 μm) and dried at 80 °C for 1 min.

2.4. Preparation of W-doped VO₂/HBPS Hydrogel Composite Films

Figure 3 is a schematic illustration of the route to prepare W-doped VO₂/HBPS hydrogel composite films. In order to prevent W-VO₂ NPs precipitation from liquid-like HBPS hydrogel, a known amount of W-VO₂ NPs were firstly added into PVP solution (2 g/L) to obtain uniform dispersion, which is a common method for the modification of VO₂ NPs [24]. After 24 h of magnetic stirring, the W-VO₂ dispersion was mixed with HBPS hydrogel. Since there was no post-processing step, the final concentration of the polymer solution was 5 and 10 g/L, respectively. Composites 1, 2, and 3 were synthesized with different addition amounts of W-VO₂ (see Supporting Information Table S1). The composite film was obtained through dropping into the “sandwich” structure (Figure 3b) to act as the function layer of the smart window. The actual contents of HBPS and W-VO₂ in these two composite films are shown in Table S1 in the Supporting Information.

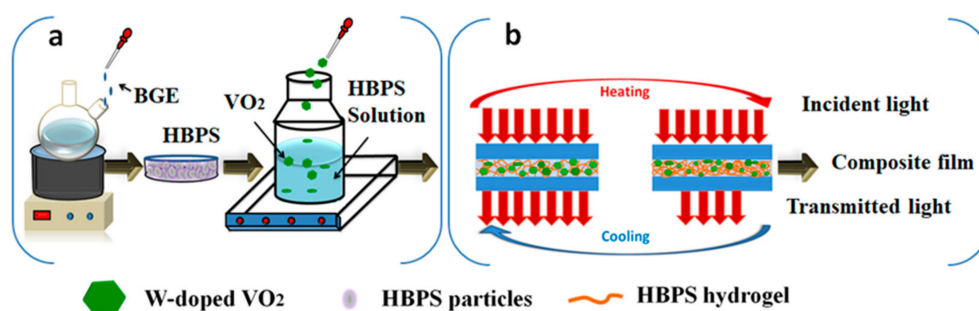


Figure 3. (a) The schematic illustration of the preparation of W-doped VO₂/HBPS composite; (b) The structure and working principle of our hybrid thermochromic film. Solar light is mostly transmitted at lower temperatures (left) and partially blocked at higher temperatures (right).

3. Characterization Methods

The transmittance spectra of HBPS films and composite films under normal incidence irradiation from 350 to 2600 nm were monitored in a sealed glass cuvette with a 3-mm thickness on the UV-vis near-IR spectrometer (U-4100, Hitachi, Ltd., Tokyo, Japan), as shown in Figure 2. The transmission data was collected using an integrating sphere. In order to assess the energy-saving performance

of all the samples, the integrated luminous transmittance (T_{lum} , 380–780 nm), IR transmittance (T_{IR} , 780–2500 nm), and solar transmittance (T_{sol} , 240–2600 nm) were calculated with Equation (2):

$$T_{lum/IR/sol, low} = \frac{\int \varphi_{lum/IR/sol, low}(\lambda) T(\lambda) d\lambda}{\int \varphi_{lum/IR/sol, low}(\lambda) \lambda d\lambda} \quad (2)$$

$T(\lambda)$ denotes spectral transmittance, and $\varphi_{lum}(\lambda)$ is the spectra sensitivity of the light-adapted eye. $\varphi_{IR}(\lambda)$ and $\varphi_{sol}(\lambda)$ are respectively the IR and solar irradiance spectrum for air mass 1.5 corresponding to the sun standing 37° above the horizon [24].

$\Delta T_{lum/IR/sol}$ was calculated by:

$$\Delta T_{lum/IR/sol} = T_{lum/IR/sol, low} - T_{lum/IR/sol, high} \quad (3)$$

where subscripts 'low' and 'high' denote low and high temperature, respectively.

$T_{lum, average}$ was calculated by:

$$T_{lum, average} = (T_{lum, low} + T_{lum, high})/2 \quad (4)$$

The response behavior of the prepared samples was monitored also by the UV-vis near-IR spectrometer with a water bath to control the system temperature. The transmittance at 1100 nm was recorded as a function of time during the switching process. Both the cooling and heating tests were conducted under the same condition. In the heating process, a sample at 15 °C was quickly moved to a water bath at 60 °C, and in the cooling process, a sample at 60 °C was rapidly transferred to a water bath at 15 °C. The heating and cooling speeds were 0.16 °C/s and 0.13 °C/s, respectively.

¹H NMR spectra were recorded on a nuclear magnetic resonance spectrometer (Varian INOVA 400, Palo Alto, CA, USA) at room temperature. For ¹H NMR characterization, HBPS were first dissolved in DMSO-d₆ containing a few drops of D₂O. Then, these HBPS samples were measured on an ¹H NMR spectrometer. Fourier transform infrared (FT-IR) spectra of HBPS samples were monitored on a FT-IR spectrometer (IR-430, JASCO, Inc., Tokyo, Japan). The LCST of HBPS was measured with a UV-vis spectrophotometer (Perkin Elmer Lambda 35, PerkinElmer, Inc., Waltham, MA, USA). The content of vanadium in the composites was determined by inductively coupled plasma (ICP Inc., Thermoelectric, IRIS Intrepid, West Chester, PA, USA). Then, the actual contents of W-doped VO₂ NPs in the composites were calculated from the ICP results (see Supporting Information Table S1).

4. Results and Discussion

4.1. Structure Analysis and Thermoresponse Properties of HBPS

As we know, the LCST value, which is defined as the temperature giving 50% of the initial transmittance, can be tailored by changing the degree of substitution of reactive groups [25]. In order to meet the different demands of smart window film applications, HBPS samples with different thermoresponse properties were obtained (Table 1). The ¹H NMR spectra clearly indicate the successful preparation of HBPS by the presence of newly emerging peaks (Figure 1a). In comparison with the unmodified starch, the new peak at 0.8 ppm (peak c) is assigned to the methyl protons of BGE. Peaks at 1.2 and 1.4 ppm and peaks between 5.1–5.4 ppm are due to the methylene group of BGE and the protons of anhydroglucose units (AGUs) of the starch, respectively [26].

Two different HBPS samples with different DS_{BGE} values (both with a HBPS content of 5 g/L), i.e., HBPS-1 and HBPS-2, were prepared to test the thermoresponsive properties of HBPS. Figure 1b shows the effect of DS_{BGE} on the phase transition behaviors of HBPS at different temperatures. The transmittance curves of the samples HBPS-1 and HBPS-2 in Figure 1b indicate that the LCST value decreased (32 to 21 °C) with increasing DS_{BGE} (0.31 to 0.42). This result clearly suggests that the hydrophobic groups can affect the thermoresponsivity of starch derivatives. When there are more

hydrophobic BGE groups being grafted on the starch backbone of HBPS, the LCST value of HBPS will be lower [26]. Since the LCST value of starch derivatives can be easily moderated over a wide range of temperature at daytime, this property can meet the various requirements of smart window systems.

4.2. Optical Transmittance Properties of HBPS Films

Figure 4 shows the solar light transmittance curves of HBPS-1 ($DS_{BGE} = 0.31$) film and HBPS-2 ($DS_{BGE} = 0.42$) film with various concentrations at 15 and 45 °C. It can be seen that below the LCST (at 15 °C), the aqueous solution of polymer appeared highly transparent and in a hydrophilic swollen state. When the temperature increased and phase transition occurred, the hydrogen bonds collapsed gradually between the polymer and water molecules, making the solution opaque. The increase of polymer concentration will lead to the formation of larger aggregates [27], resulting in the decrease in the transmittance of the HBPS-1 and HBPS-2 films in both the visible and IR ranges.

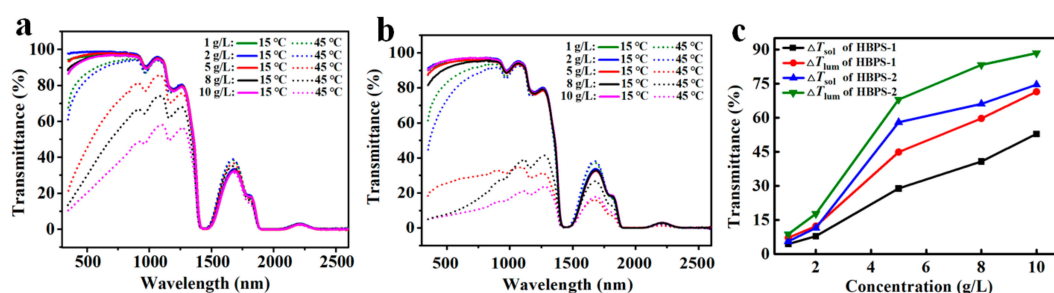


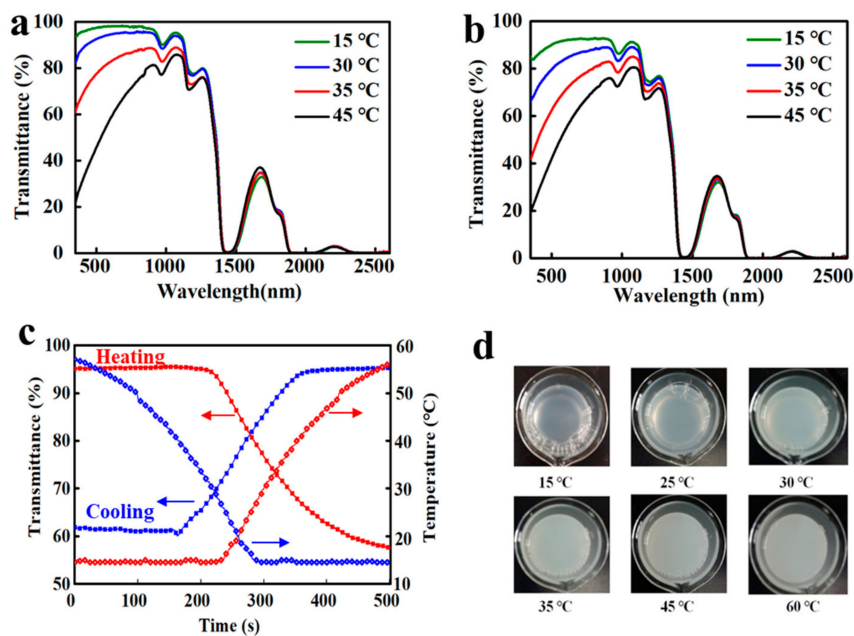
Figure 4. Transmittance curves of (a) HBPS-1 and (b) HBPS-2 with various concentrations between 1–10 g/L at 15–45 °C; (c) A summary for the optical performance of temperature-responsive starch derivative samples (HBPS-1 and HBPS-2) under different concentrations (HBPS-1 and HBPS-2 have different substitution degrees).

As illustrated in Figure 4a and Table 2, the $T_{lum,high}$ of HBPS-1 film slightly decreased with increased HBPS concentration after phase transition, but still remained at a high level of 49.6% at a high concentration of 10 g/L. For the transmittance curves of HBPS-2 film (Figure 4b), there existed a large contrast in both the visible and IR rangess (e.g., $T_{lum,high}$ of HBPS-2 with 5 g/L was 28.9%). The same trend can be seen in the plots of ΔT_{lum} (%) and ΔT_{sol} (%) against concentration for HBPS-1 film and HBPS-2 film (Figure 4c). At each concentration, both the values of ΔT_{lum} (%) and ΔT_{sol} (%) for the HBPS-2 film were higher than those of the HBPS-1 film. However, this high ΔT_{lum} (%) of the HBPS-2 film will lead to a low luminous transmission after phase transition (e.g., $T_{lum,high}$ of HBPS-2 film with 10 g/L was only 7.8%). Compared with the HBPS-2 film, the HBPS-1 film was more suitable for smart windows with higher luminous transmission, and the LCST of the HBPS-1 film was 32 °C, which is also close to the phase transition temperature of W-doped VO_2 (M) (39 °C, see Supporting Information Figure S1). Herein, HBPS-1 films with concentrations of 5 g/L and 10 g/L were opted for further experiments.

The optical properties of HBPS-1 film with different contents (5 and 10 g/L) were briefly investigated. As presented in Figure 5a,b and Table 2, the increase of HBPS content has a slight effect on both T_{lum} and ΔT_{sol} values. The T_{lum} value of the HBPS-1 film reduced from 97.9% to 95.8% with increased HBPS-1 contents. The phase transition speed test was also conducted. Traditionally, a high-phase transition speed is necessary for smart window applications. On the other hand, controlling the transmittance in a stepwise manner on demand has a lot of advantages [27], such as for example, reducing the unnecessary energy consumption and a suitable visible transmittance for views. As shown in Figure 5c, the phase transition time period of HBPS-1 (10 g/L) was around 300 s, which is higher than that of the PNIPAm microgel to some extent. This long phase time period of HBPS-1 film will cause the transmittance to change gradually (Figure 5d), thus making it favorable to realize the stepwise solar control on practical demand.

Table 2. Comparison of the optical properties between composites 1, 2, and 3 and poly (*N*-isopropylacrylamide) (PNIPAm) hydrogel, VO₂/hydrogel hybrid, and VO₂.

Sample	$T_{lum, low}$ (%)	$T_{lum, high}$ (%)	ΔT_{lum} (%)	$T_{lum, average}$ (%)	ΔT_{IR} (%)	ΔT_{sol} (%)
PNIPAm hydrogel [11]	88.5	58.8	29.7	73.6	9.5	21.4
VO ₂ /hydrogel [13]	82.1	43.2	38.9	62.6	29.9	34.7
VO ₂ [9]	45.6	40	5.6	42.8	—	22.3
HBPS-1 (5 g/L)	97.9	53.1	44.8	75.5	5.0	28.9
HBPS-1 (10 g/L)	95.8	49.6	46.2	72.7	6.3	31.0
HBPS-2 (5 g/L)	94.9	28.9	68.0	60.9	20.7	58.0
HBPS-2 (10 g/L)	96.2	7.8	88.4	52.0	26.2	74.6
Composite 1	88.2	56.9	37.6	72.6	11.6	24.7
Composite 2	92.0	43.6	48.5	67.8	15.1	32.5
Composite 3	78.7	29.0	49.8	53.9	8.5	34.3

**Figure 5.** Optical transmittance spectra of (a) HBPS-1 (5 g/L) and (b) HBPS-1 (10 g/L) at different temperatures from 15 to 45 °C; (c) Temperature and transmittance (at 1100 nm) changes as a function of time through cooling or heating across LCST for HBPS-1 (10 g/L). The heating speed was 0.16 °C/s, and the cooling speed is 0.13 °C/s; (d) Pictures of HBPS-1 (10 g/L) at various temperatures.

4.3. Optical Transmittance Properties of Composite Films

The transmittance spectra and values of $T_{lum, low}$, ΔT_{lum} , ΔT_{IR} , and ΔT_{sol} of different composites (composites 1, 2, and 3) with different contents of W-doped VO₂ NPs were investigated. As shown in Figure 6 and Table 2, the luminous transmittance at 25 °C and the value of $T_{lum, average}$ were both reduced with increased W-doped VO₂ NPs content. Due to the increased ΔT_{IR} and ΔT_{lum} values, the value of the solar modulation was augmented from 24.7% of Composite 1 to 32.5% of Composite 2 and 34.3% of Composite 3. For further investigation of the optical performance of the composites, composites 2 and 3 were chosen and compared to HBPS and the W-doped VO₂/PU film.

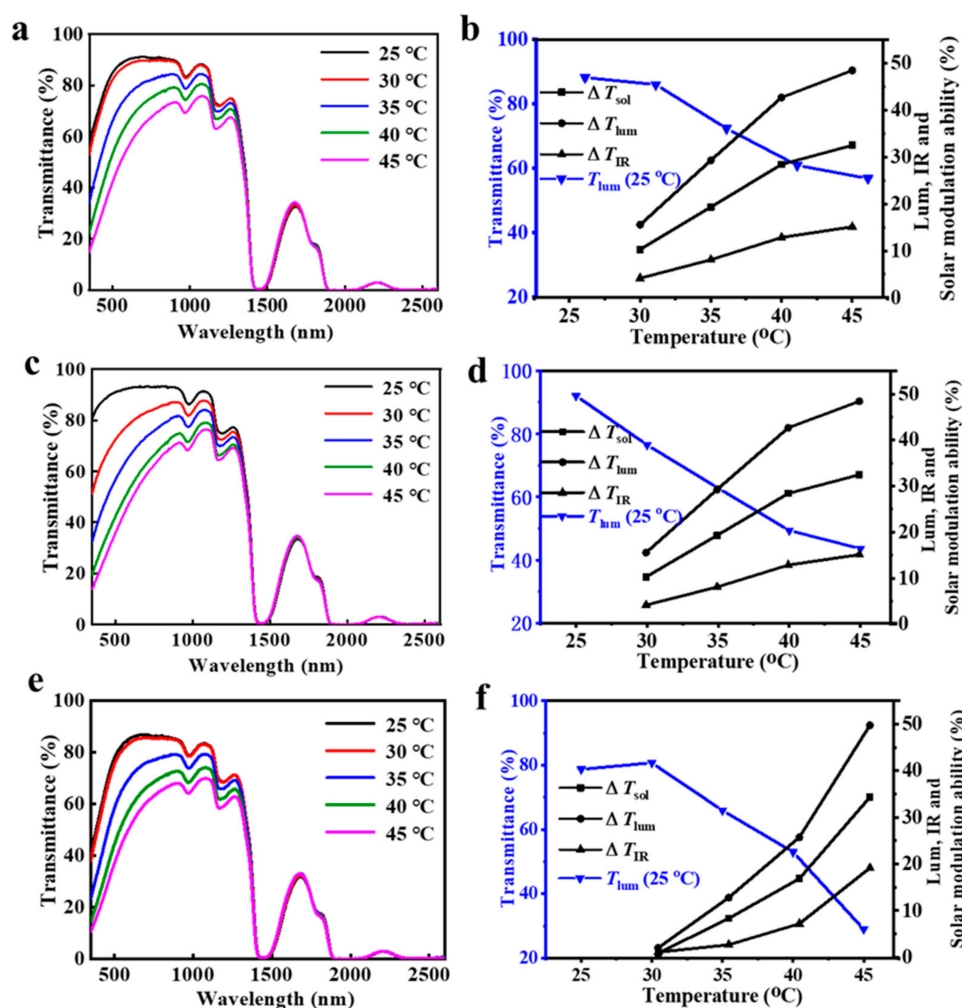


Figure 6. UV-vis near-IR spectra of (a) Composite 1, (c) Composite 2, (e) Composite 3 at different temperatures from 15 to 45 °C; changes of T_{lum} , ΔT_{sol} , ΔT_{IR} , and ΔT_{lum} of (b) Composite 1, (d) Composite 2, and (f) Composite 3.

The transmittance spectra of the pure HBPS-1 film (5 g/L), W-doped VO₂/PU film, Composite 2 film, and Composite 3 film are shown in Figure 7a. The ΔT_{lum} value of the pure HBPS-1 (5 g/L) film was high (44.8%), thus leading to high solar modulation properties (28.9%). However, the IR modulation property of the pure HBPS-1 (5 g/L) film was low. As we know, VO₂ has large transmission contrast in the IR region, so dispersing VO₂ NPs into the polymer matrix will enhance the optical performance. Due to the large contrast in the IR range of around 1250 nm, the existence of W-doped VO₂ improves the solar modulation property of composite films. As shown in Figure 5b and Table 2, the ΔT_{IR} (%) value increased from 5.0 to 8.5 with an increase in W-doped VO₂ concentration, and the solar modulation property was also improved from 28.9% to 34.3%. Although increasing the concentration of W-doped VO₂ lowered the transmittance at both 20 and 45 °C, the obtained composite films were superior in the modulation ability of the visible range and the infrared range. The pleasing performance of Composite 2 is favorable for smart window systems. Comparing with PNIPAM hydrogel smart window systems, the Composite 2 film has a much higher ΔT_{sol} value (32.5% versus 21.4%). The VO₂/PNIPAM hydrogel was also compared with the Composite 2 film in Table 2, confirming that the Composite 2 film has a slightly higher $T_{lum, average}$ (%) value with a slightly lower ΔT_{sol} (%) value (Table 2).

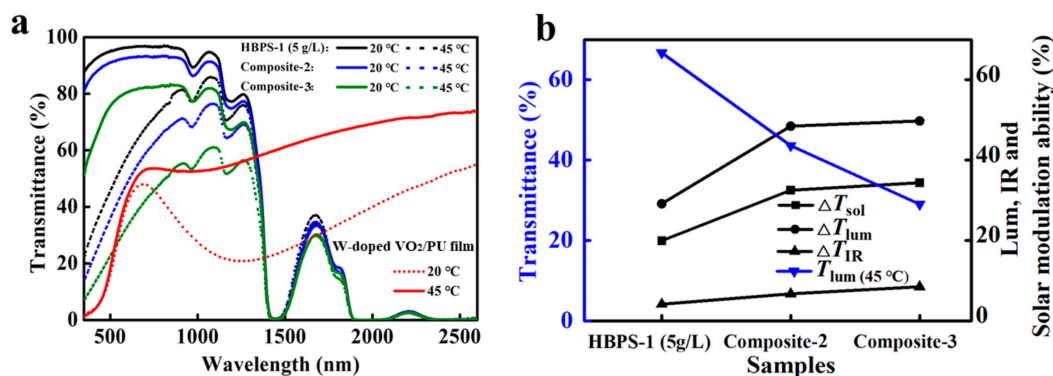


Figure 7. (a) UV-vis near-IR spectra of films of W-doped VO₂ (M)/PU with 2-3 μm thickness (red solid and dashed lines), HBPS-1 (5 g/L), Composite 1 and Composite 2 at 20 and 45 °C; (b) Changes of T_{lum} , ΔT_{sol} , ΔT_{IR} , and ΔT_{lum} for films of HBPS-1 (5 g/L), Composite 2, and Composite 3.

4.4. Cyclic Stability of Composite Films

Since the high W-doped VO₂ NP loading capacity could cause sedimentation problems, Composite 3 was chosen for the durability test. As shown in Figure 8, only slight fluctuations in the values of ΔT_{sol} and T_{lum} were observed after eight cycles of measurement. Considering the satisfying performance stability, the suitable transition temperature, and the best optical performance exhibited by the composites prepared in this work, they should be ideal candidates for the thermochromic smart window system.

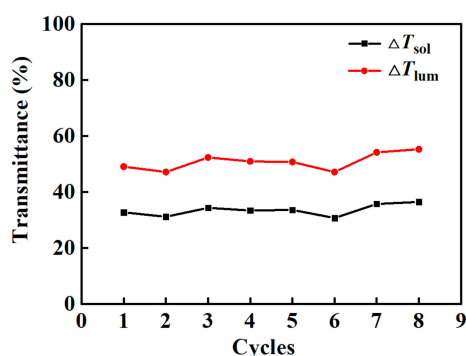


Figure 8. Changes in light transmittance at 1100 nm in the durability test of Composite 3 between 20–45 °C.

5. Conclusions

In this work, for the first time, a W-doped VO₂/starch derivative thermochromic hybrid film was obtained. Firstly, we prepared pure W-doped VO₂ (M) NPs and pure HBPS hydrogel both with a low phase transition temperature (39 and 32 °C respectively). Due to these two similar and low phase transition temperatures, the near-room temperature composite thermochromic film was obtained by incorporating W-doped VO₂ (M) with HBPS hydrogel. It was found that these composite films with W-doped VO₂ (M) NPs show excellent optical performance with improved solar modulation property ($T_{sol} = 34.3\%$) and luminous transmittance (T_{lum} , average % = 53.9%).

Supplementary Materials: The Supplementary Materials are available online at <http://www.mdpi.com/2079-4991/9/7/970/s1>. Figure S1: (a) XRD results of the VO₂(M) NPs and the W-VO₂(M) NPs; (b) DSC curve as function of temperature upon heating of W-doped VO₂(M) NPs, Figure S2: (a) Diameter of W-doped VO₂ NPs before (dash line) and after (solid line) grinding, and the insert picture shows the W-doped VO₂ suspension with white zirconia pellets; (b) TEM image of Composite-2, Figure S3: Hysteresis loop for the temperature-dependent transmittance of the Composite-2 at a wavelength of 550 nm, Table S1: Description of the two different organic-inorganic hybrid thermochromic films investigated in this work, Table S2: Comparison of my hybrid sample with other thermochromic materials (note: “–” means data not available).

Author Contributions: Conceptualization Y.G. and X.G.; Data curation Y.W.; Formal analysis J.W.; Funding acquisition L.L.; Investigation Y.W.; Methodology K.Z. and Y.S.; Supervision Y.G. and X.G.; Writing—original draft Y.W.; Writing—review & editing F.Z., Y.G. and X.G.

Funding: We gratefully thank the financial support from the NSFC Grants (51761135128 and 51773061), Key Scientific and Technological Project of Xinjiang Bingtuan (2018AB025), and the Fundamental Research Funds for the Central Universities (22221818010 and 222201917013).

Conflicts of Interest: The authors declare no conflict of interest.

References

1. Wang, Y.; Wang, J.; Zhang, K.; Li, L.; Chen, Z.; Gao, Y.; Guo, X. Application of thermochromic hydrogels as novel materials of energy chemical engineering in smart window. *J. East China Univ. Sci. Technol.* **2018**, *44*, 1–8.
2. Cui, Y.; Ke, Y.; Liu, C.; Chen, Z.; Wang, N.; Zhang, L.; Zhou, Y.; Wang, S.; Gao, Y.; Long, Y. Thermochromic VO₂ for Energy-Efficient Smart Windows. *Joule* **2018**, *2*, 1–40. [[CrossRef](#)]
3. Chen, Z.; Gao, Y.; Kang, L.; Du, J.; Zhang, Z.; Luo, H.; Miao, H.; Tan, G. VO₂-based double-layered films for smart windows: Optical design, all-solution preparation and improved properties. *Sol. Energy Mater. Sol. Cells* **2011**, *95*, 2677–2684. [[CrossRef](#)]
4. Ke, Y.; Zhou, C.; Zhou, Y.; Wang, S.; Chan, S.H.; Long, Y. Emerging Thermal-Responsive Materials and Integrated Techniques Targeting the Energy-Efficient Smart Window Application. *Adv. Funct. Mater.* **2018**, *28*, 1800113. [[CrossRef](#)]
5. Azens, A.; Granqvist, C. Electrochromic smart windows: Energy efficiency and device aspects. *J. Solid State Electrochem.* **2003**, *64*, 64–68. [[CrossRef](#)]
6. Wittwer, V.; Datz, M.; Ell, J.; Georg, A.; Graf, W.; Walze, G. Gasochromic windows. *Sol. Energy Mater. Sol. Cells* **2004**, *84*, 305–314. [[CrossRef](#)]
7. Kang, L.; Gao, Y.; Luo, H.; Chen, Z.; Du, J.; Zhang, Z. Nanoporous thermochromic VO₂ films with low optical constants, enhanced luminous transmittance and thermochromic properties. *ACS Appl. Mater. Interfaces* **2011**, *3*, 135–138. [[CrossRef](#)]
8. Feng, W.; Zou, L.; Gao, G.; Wu, G.; Shen, J.; Li, W. Gasochromic smart window: Optical and thermal properties, energy simulation and feasibility analysis. *Sol. Energy Mater. Sol. Cells* **2016**, *144*, 316–323. [[CrossRef](#)]
9. Drosos, C.; Vernardou, D. Perspectives of energy materials grown by APCVD. *Sol. Energy Mater. Sol. Cells* **2015**, *140*, 1–8. [[CrossRef](#)]
10. Louloudakis, D.; Vernardou, D.; Spanakis, E.; Katsarakis, N.; Koudoumas, E. Thermochromic vanadium oxide coatings grown by APCVD at low temperatures. *Phys. Procedia* **2013**, *46*, 137–141. [[CrossRef](#)]
11. Chen, Z.; Gao, Y.; Kang, L.; Cao, C.; Chen, S.; Luo, H. Fine crystalline VO₂ nanoparticles: Synthesis, abnormal phase transition temperatures and excellent optical properties of a derived VO₂ nanocomposite foil. *J. Mater. Chem. A* **2014**, *2*, 2718–2727. [[CrossRef](#)]
12. Zhang, Q.; Hoogenboom, R. Polymers with upper critical solution temperature behavior in alcohol/water solvent mixtures. *Prog. Polym. Sci.* **2015**, *48*, 122–142. [[CrossRef](#)]
13. Zhou, Y.; Cai, Y.; Hu, X.; Long, Y. Temperature-responsive hydrogel with ultra-large solar modulation and high luminous transmission for “smart window” applications. *J. Mater. Chem. A* **2014**, *2*, 13550–13555. [[CrossRef](#)]
14. Wang, M.; Gao, Y.; Cao, C.; Chen, K.; Wen, Y.; Fang, D.; Li, L.; Guo, X. Binary solvent colloids of thermosensitive poly (n-isopropylacrylamide) microgel for smart windows. *Ind. Eng. Chem. Res.* **2014**, *53*, 18462–18472. [[CrossRef](#)]
15. Zhou, Y.; Cai, Y.; Hu, X.; Long, Y. VO₂/hydrogel hybrid nanothermochromic material with ultra-high solar modulation and luminous transmission. *J. Mater. Chem. A* **2015**, *3*, 1121–1126. [[CrossRef](#)]
16. Zhu, J.; Huang, A.; Ma, H.; Chen, Y.; Zhang, S.; Ji, S.; Bao, S.; Jin, P. Hybrid films of VO₂ nanoparticles and a nickel(ii)-based ligand exchange thermochromic system: Excellent optical performance with a temperature responsive colour change. *New J. Chem.* **2017**, *41*, 830–835. [[CrossRef](#)]

17. Houska, J.; Kolenaty, D.; Vlcek, J.; Barta, T.; Rezek, J.; Cerstvy, R. Significant improvement of the performance of $ZrO_2/V_{1-x}W_xO_2/ZrO_2$ thermochromic coatings by utilizing a second-order interference. *Sol. Energy Mater. Sol. Cells* **2019**, *191*, 365–371. [[CrossRef](#)]
18. Peng, Z.; Jiang, W.; Liu, H. Synthesis and electrical properties of tungsten-doped vanadium dioxide nanopowders by thermolysis. *J. Phys. Chem. C* **2007**, *111*, 1119–1122. [[CrossRef](#)]
19. Hu, L.; Tao, H.; Chen, G.; Pan, R.; Wan, M.; Xiong, D.; Zhao, X. Porous W-doped VO_2 films with simultaneously enhanced visible transparency and thermochromic properties. *J. Sol Gel Sci. Technol.* **2016**, *77*, 85–93. [[CrossRef](#)]
20. Zhang, K.; Shi, Y.; Wu, L.; Chen, L.; Wei, T.; Jia, X.; Chen, Z.; Li, M.; Xu, Y.; Wang, Y.; et al. Thermo- and pH-responsive starch derivatives for smart window. *Carbohydr. Polym.* **2018**, *196*, 209–216. [[CrossRef](#)]
21. Wang, Y.; Shi, Y.; Xu, M.; Wu, L.; Jia, X.; Wei, T.; Zhang, S.; Guo, X. Smart flocculant with temperature and pH response derived from starch. *RSC Adv.* **2016**, *6*, 44383–44391. [[CrossRef](#)]
22. Ju, B.; Yan, D.; Zhang, S. Micelles self-assembled from thermoresponsive 2-hydroxy-3-butoxypropyl starches for drug delivery. *Carbohydr. Polym.* **2012**, *87*, 1404–1409. [[CrossRef](#)]
23. Shen, N.; Bong, B.; Cao, C.; Chen, Z.; Liu, J.; Luo, H.; Gao, Y. Lowered phase transition temperature and excellent solar heat shielding properties of well-crystallized VO_2 by W doping. *Phys. Chem. Chem. Phys.* **2016**, *18*, 28010–28017. [[CrossRef](#)]
24. Gao, Y.; Wang, S.; Luo, H.; Dai, L.; Cao, C.; Liu, Y.; Chen, Z.; Kanehira, M. Enhanced chemical stability of VO_2 nanoparticles by the formation of SiO_2/VO_2 core/shell structures and the application to transparent and flexible VO_2 -based composite foils with excellent thermochromic properties for solar heat control. *Energy Environ. Sci.* **2012**, *5*, 6104–6110. [[CrossRef](#)]
25. Gao, M.; Jia, X.; Kuang, G.; Li, Y.; Liang, D.; Wei, Y. Thermo- and pH-Responsive Dendronized Copolymers of Styrene and Maleic Anhydride Pendant with Poly(amidoamine) Dendrons as Side Groups. *Macromolecules* **2009**, *42*, 4273–4281. [[CrossRef](#)]
26. Ju, B.; Zhang, C.; Zhang, S. Thermoresponsive starch derivatives with widely tuned LCSTs by introducing short oligo(ethylene glycol) spacers. *Carbohydr. Polym.* **2014**, *108*, 307–312. [[CrossRef](#)]
27. Lee, E.; Kim, D.; Yoon, J. Stepwise Activation of Switchable Glazing by Compositional Gradient of Copolymers. *ACS Appl. Mater. Interfaces* **2016**, *8*, 26359–26364. [[CrossRef](#)]



© 2019 by the authors. Licensee MDPI, Basel, Switzerland. This article is an open access article distributed under the terms and conditions of the Creative Commons Attribution (CC BY) license (<http://creativecommons.org/licenses/by/4.0/>).